frontiers | Frontiers in Ecology and Evolution

TYPE Original Research
PUBLISHED 22 February 2024
DOI 10.3389/fevo.2024.1320539

OPEN ACCESS

EDITED BY
Laurent Marquer,
University of Innsbruck, Austria

REVIEWED BY
John Dodson,
Chinese Academy of Sciences (CAS), China
Harry Dowsett,
United States Department of the Interior, United States
Honghao Niu,
Jilin University, China

*CORRESPONDENCE
Xiangmin Zheng
xmzheng@re.ecnu.edu.cn
Peng Qian
zgw3916@163.com

†These authors share first authorship

RECEIVED 12 October 2023
ACCEPTED 05 February 2024
PUBLISHED 22 February 2024

CITATION
Wang Z, Wang C, Zhang Y, Cheng Y, Ren S, Yi C, Wang H, Zhou L, Qian P and Zheng X (2024) Fire dynamics and driving mechanisms on the Eastern Coast of China since the Late Pleistocene: evidence from charcoal records on Shengshan Island.
Front. Ecol. Evol. 12:1320539.
doi: 10.3389/fevo.2024.1320539

Fire dynamics and driving mechanisms on the Eastern Coast of China since the Late Pleistocene: evidence from charcoal records on Shengshan Island

Zhigang Wang[1,2†], Cuiping Wang[1†], Yao Zhang[3], Yuanyu Cheng[4], Shaofang Ren[1], Chengxin Yi[1], Hui Wang[1], Limin Zhou[1], Peng Qian[5*] and Xiangmin Zheng[1*]

[1]The Key Laboratory of Geo-information Science of Ministry of Education, East China Normal University, Shanghai, China, [2]Polar Terrestrial Environmental Systems Research Group, Alfred Wegener Institute Helmholtz Centre for Polar and Marine Research, Potsdam, Germany, [3]College of Geography and Environmental Sciences, Zhejiang Normal University, Jinhua, China, [4]Department of Biology, McGill University, Montreal, QC, Canada, [5]The School of Geography, Nantong University, Nantong, China

Fires play a significant role in ecosystems, exerting a profound influence on climate, vegetation, and geochemical cycles, while being reciprocally affected by these factors. The reconstruction of past fire events serves as a valuable window into understanding environmental changes over time. To investigate the history of ancient fires on the Eastern Coast of China, we conducted the first charcoal analysis on a loess profile of Shengshan Island (East China Sea). Along with other biological and geochemical proxies, we successfully reconstructed the ancient fire dynamics and elucidated their driving mechanisms in this region since the Late Pleistocene. Our initial findings revealed a peak in charcoal concentration during the 60-50 ka period, but after calibrating for sedimentation rate, the concentration significantly decreased. Fire activities remained weak during 50-30 ka, likely due to the scarcity of combustible materials. Between 30-12 ka, fires were frequent in the early period, while gradually diminishing during the later stage. Dry climate and dense vegetation likely attributed to frequent fires in early period, while some extreme events (e.g., sudden change in temperature) may have decreased the fire frequency in later period. The Holocene (began ~12 ka) evidenced the most frequent fire events as a high charcoal concentration was recorded, likely caused by human activities. After comparing our findings with other paleoecological records from surrounding areas, we confirmed the accuracy of our reconstruction of ancient fires. This reconstruction captures

not only local shifts but also broader regional changes. Overall, our study highlights the importance of calibrating sedimentation rate in charcoal profiles, while also contributing to an enhanced understanding of environmental changes along the Eastern Coast of China since the Late Pleistocene.

KEYWORDS

Shengshan Island, Late Pleistocene, ancient fires, charcoal, climate change

1 Introduction

Fires not only threaten human life and safety but also exert strong influences on global ecosystem patterns and processes, including vegetation distribution and structure, carbon cycles, and climate feedbacks (Scott and Glasspool, 2006; Bowman et al., 2009). They produce gases and aerosols that influence climate, burn vegetation, as well as alter geochemical cycles (Ramanathan et al., 2001; Santín et al., 2016). Meanwhile, the occurrence of fires is also influenced by changes in climate (temperature and humidity), vegetation (type and density), and geochemical cycling in return (Haberle et al., 2001; Cui et al., 2013; Leys and Carcaillet, 2016; Bobek et al., 2018; Leys et al., 2018; Lian, 2019; Min et al., 2020; Molinari et al., 2020). Therefore, studying fire dynamics and their driving mechanisms over geological timescale is an important tool to reconstruct ancient climate and vegetation changes, and it can provide a reference for future ecological conservation and sustainable development (Power et al., 2008; Xue et al., 2018).

Fire activities can be measured via different parameters, such as intensity, frequency, extent, and type (Gill, 1977; Bond and Keeley, 2005). There are various types of indicators available for fire reconstruction, such as tree–ring fire scar, charcoal, black carbon, polycyclic aromatic hydrocarbons and levoglucosan (MacDonald et al., 1991; Millspaugh and Whitlock, 1995; Daniau et al., 2010). Among these indicators, charcoal, a carbonaceous material produced by incomplete combustion of organic matters (Patterson et al., 1987; Whitlock et al., 2003), is often well-preserved in sediments over long periods and thus serves as a reliable proxy of ancient fire events (Patterson et al., 1987; Lv et al., 2002; Hu et al., 2019). In recent years, charcoal has been widely applied in reconstructing fire events spanning extensive spatial and temporal scales (MacDonald et al., 1991; Hoetzel et al., 2013; Miao et al., 2016; Shi et al., 2020; Hui et al., 2021; Moore et al., 2022). These studies primarily use charcoal concentration, particle size, and morphology to indicate the frequency of fire events (Clark, 1988; Umbanhowar and Mcgrath, 1998). Charcoal concentration serves as an indicator of fire frequency: elevated charcoal concentrations correspond to more frequent occurrences (Guo et al., 2011; Xin and Yiyin, 2015). Charcoal particle size can help indicate the fire event proximity: larger particles often indicate local fire events, while smaller particles likely suggest regional events (McElwain, 1998; Moore et al., 2022). Lastly, charcoal morphology can provide insights into the fuels, especially the types of vegetation burnt (Jensen et al., 2007; Pereboom et al., 2020). For instance, the length:width ratio of the charcoal particles is a common measurement to distinguish whether the fuels originate from woody or herbaceous sources (Enache and Cumming, 2006; Crawford and Belcher, 2014; Leys et al., 2017).

Situated in the East China Sea, Shengshan Island (SSD) stands as one of the outermost islands within the Zhoushan Islands (Figure 1), and the loess on SSD marks the easternmost aeolian dust landscape in China (Wu et al., 2023). Unlike the extensively studied Loess Plateau loess, SSD loess is shaped by not only East Asian monsoon but also sea level changes. This dual influence underscores its significance as a vital component in reconstructing the paleoenvironment of Eastern China. Prior research has analyzed the SSD loess profile regarding its sedimentology (Zheng and Liu, 2006; Ren et al., 2018), geochemistry (Qian et al., 2018), micropaleontology (Zheng, 2002), magnetic properties (Liu et al., 2020), and geochronology (Wu et al., 2023). However, there exists a significant knowledge gap regarding ancient fire history on SSD.

In this study, we provide the first analysis on charcoal records of SSD to reconstruct the fire events in this region since the late Pleistocene. Combined with biological proxies (TOC and $\delta^{13}C_{org}$) and geochemical indicators (magnetic susceptibility and Rb/Sr ratio), we inferred past changes in vegetation and climate. We identified sedimentation rate to be an important factor affecting the charcoal concentration and calibrated its impact. Further, we gathered environmental data from other studies, including solar radiation (July, 30°N) (Ding and Liu, 1998), global CO_2 concentration (Monnin et al., 2001; Pépin et al., 2001; Siegenthaler et al., 2005), and Sulu Sea deep-sea oxygen isotope ($\delta^{18}O$) (Linsley, 1996), aiming to identify the driving forces behind the changes in charcoal concentration. Additionally, to demonstrate the accuracy of our results, we compared our findings with other paleoecological records derived from surrounding areas, including Lake Biwa (Inoue et al., 2018), Core YZ07 (Ye et al., 2024), HML (Zhang et al., 2020), Middle Okinawa Trough (Zheng et al., 2011), KCES-1 (Chen et al., 2017). In the end, we assessed and discussed the interactions between fire events, vegetation, climate, and human activities. Overall, our study contributes to an enhanced understanding of environmental changes along the Eastern Coast of China since the Late Pleistocene.

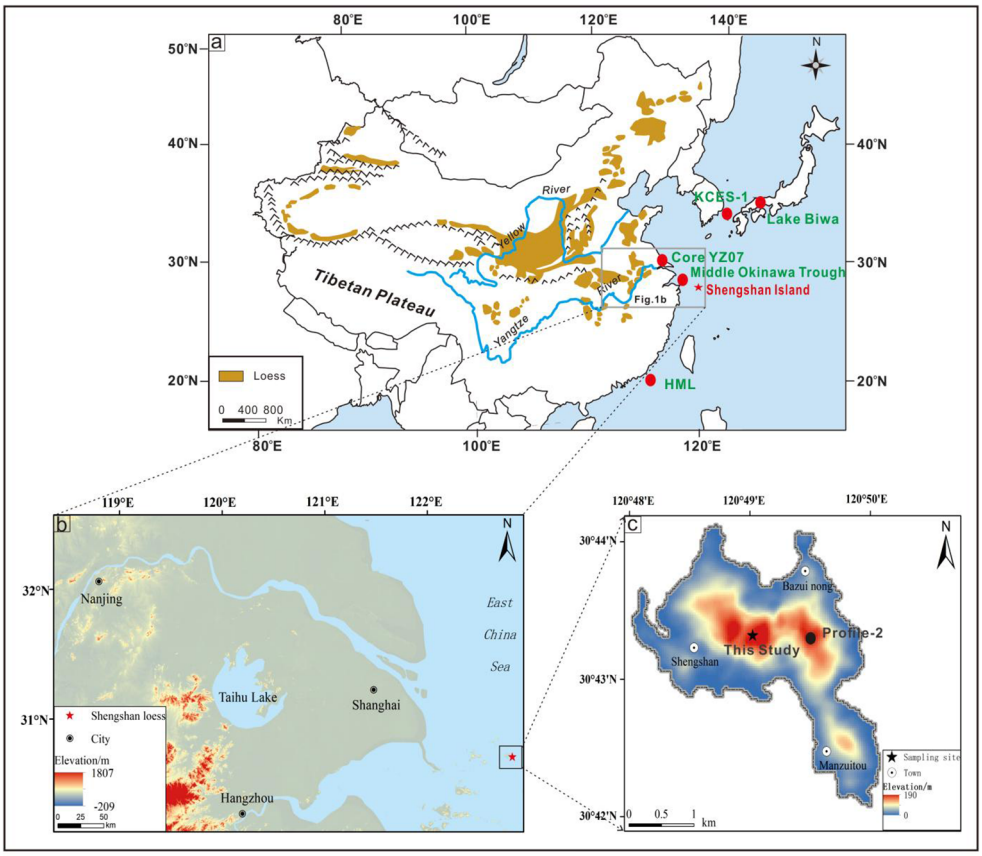

FIGURE 1
(A) Loess distribution in China, with red points showing the locations of relevant paleoecological studies (compared with our results): Lake Biwa (Inoue et al., 2018), Core YZ07 (Ye et al., 2024), HML (Zhang et al., 2020), Middle Okinawa Trough (Zheng et al., 2011), KCES-1 (Chen et al., 2017); **(B)** Location of Shengshan Island loess profile in eastern China; **(C)** Sampling points of Shengshan Island loess profiles.

2 Study area

Shengshan Island (30.44°N, 122.49°E), located at the estuary of Yangtze River, is the eastern most island in the China Eastern Sea (Figure 1). Spanning 3.3 km from south to north and 2.6 km from east to west, it covers a total surface area of 4.22 km², boasting a coastline extending 19.26 km. Shengshan Island is mainly composed of granite, with most areas having bedrock directly exposed on the surface. The island topography is characterized by low mountains and hills, with the highest peak, Mount Chenqian, reaching an elevation of 213 m above sea level (Figure 1C).

Shengshan Island has a subtropical monsoon climate. In summer, it is influenced by the southeast monsoon and typhoons, resulting in high temperature and abundant rainfall. In winter, it is affected by the Mongolian-Siberian high-pressure system and the northwest monsoon, leading to a cold and dry climate. The annual average temperature is ~ 16.4°C, while annual average precipitation is ~ 1072.5 mm.

The island is mainly covered by evergreen broadleaved trees, including *Commersonia*, *Quercus*, and *Ilex*. Neighboring islands are mainly covered by herbaceous trees and grass (e.g., *Ficus erecta*), as well as some deciduous broadleaved trees (e.g., *Paulownia tomentosa)* and patches of coniferous trees such as *Pinus* and *Cunninghamia* (Zheng and Liu, 2006; Ren et al., 2018). Overall, Shengshan Island and its surrounding islands have a high vegetation coverage.

Currently, the permanent population on Shengsi Island is about 10,000 people, with a long history of development. According to cultural relics and historical records (shengsi.gov.cn, n.d.), humans have inhabited the area since the Neolithic era (10,000-3,500 BCE).

3 Materials and methods

3.1 Sample collection

A loess profile from Shengshan Island was collected from the northeastern slope of Mountain Chenqian (the highest peak on the island) at ~150 m a.s.l. (30.730°N, 122.817°E, Figure 1C). The loess spans ~280 cm in depth and displays three distinct layers (Table 1) based on visual assessment on site (Figure 2). Considering the potential impact of recent human activities, we collected samples starting from 10 cm below the surface. Subsampling was done at each 1-cm interval, and in total 270 samples were collected.

TABLE 1 Layer description of the Shengshan Island loess profile.

Depth (cm)	Layer	Description
0-40	Modern tillage layer	Dark black-grey color, loose structure, well-developed plant root system, rich humus content, and no apparent bedding
40-275	Loess layer	Yellow-brown color, fine grain size, porous and loose texture, many mixed calcareous and Fe-Mn nodules, scarce plant roots
275-280	Bedrock weathered layer	Unconformable contact with the overlaying loess layer, obvious mixture of weathered granite and loess sediments

3.2 Optically stimulated luminescence dating

Optically stimulated luminescence (OSL) dating was used to estimate the age of loess deposits. OSL dating samples were gathered at depths of 10 cm, 100 cm, 150 cm, and 250 cm (Figure 2). The samples were stored in stainless steel tubes measuring 20 cm in length and 5 cm in diameter. Both ends of the tubes were covered with black plastic bags to prevent exposure to light during collection, transportation, storage, and experimental processes. Moisture within the samples was also effectively preserved.

OSL measurements were conducted in a dark room with red light available, using a Riso TL/OSL automated luminescence meter (model DA-20-C/D). Samples potentially exposed to light were removed. The remaining samples underwent sequential soaking in 10% HCL and 30% H_2O_2 to eliminate carbonates and organic matter. Wet sieving was performed to extract 90-150 μm quartz particles, followed by a 40-minute treatment with 40% HF to remove feldspar. Infrared inspection ensured the absence of feldspar contamination in the quartz. Finally, the sample was dry-sieved to obtain pure quartz particles (Lai, 2006). Then an equivalent dose (De) of the extracted quartz was then determined following the Single Aliquot Regenerative-Dose (SAR) protocol (Murray and Wintle, 2000). Radioactive isotope concentrations (U, Th, and K) in the samples were measured via a neutron activation analysis (NAA). The cosmic ray dose rate was calculated using parameters provided by Prescott and Hutton, and the dose rate was finally calculated using Aitken's formula and parameters. The "DRACv1.2" online program was used to calculate the final ages (Durcan et al., 2015).

3.3 Charcoal extraction and analysis

27 samples, spaced at intervals of 10 cm, were collected for charcoal extraction and analysis. All samples were treated according to the modified protocol palynological methods: acid digestion followed heavy liquid flotation (Nakagawa et al., 1998; Tan et al., 2011). In brief, about 30 g of air-dried sample was added with two pellets of *Lycopodium clavatum* spores (10,315 spores per pellet (Stockmarr, 1971; Maher, 1981). Then each sample was treated with ~ 200 ml of 10% HCl, and after thorough reaction, they were washed by distilled water to reach a neutral pH. Subsequently, the samples were dried by heating them in a water bath at 80°C. Following this, ~ 300 ml of 40% HF were added to each sample, once again undergoing thorough reaction and subsequent washing to neutrality. After acid digestions, heavy liquid (density: 1.98 g/cm^3) equivalent to three times the volume of the remaining sample, was added to each sample. Prior to centrifugation (at 3,000 xg for 5 minutes), the samples were thoroughly mixed. Then, the supernatant was processed through a 200-μm metal sieve and a 10 μm nylon mesh to concentrate the charcoal particles, and collected in the storage tube. Lastly, the extracted charcoal samples were mounted on microscopic slides for observation.

Charcoal particles were enumerated using a light microscope at 40X magnification (Olympus BX43), and their diameters were measured utilizing an eyepiece graticule. Charcoal particles are

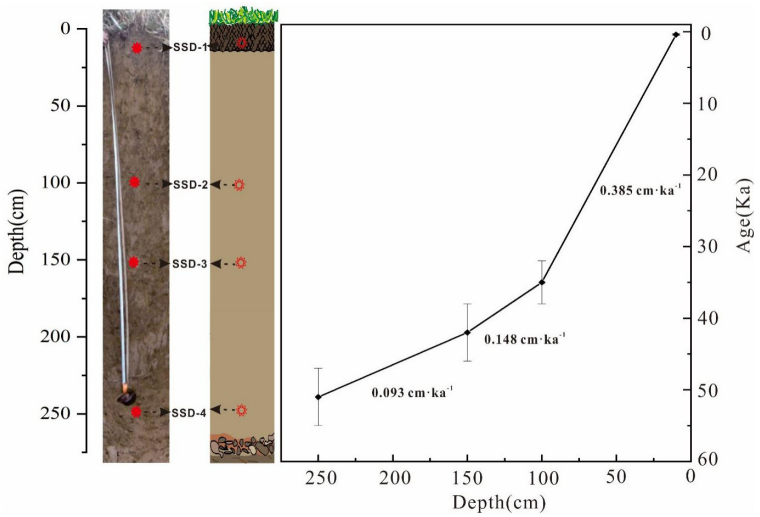

FIGURE 2
Left: Shengshan Island loess profile photo and profile description, with red marks showing the sampling points of OSL dating. Right: OSL age versus sediment depth of the Shengshan Island loess profile, with sediment accumulation rate (cm/ka) indicated.

typically distinguished by their opacity and angularity, appearing as jet-black, opaque, and angular entities (Figure 3). In contrast, other opaques, such as mineral fragments, insect cuticles, and undigested plant fragments, typically manifest as clear or brown amorphous weakly structured particles or possess a distinct shape. Therefore, differentiation between charcoal and other opaques is often feasible based on their color and shape (Patterson et al., 1987). At least 300 charcoal particles with the diameter >10 μm were counted per sample (Wang et al., 2020). Charcoals were classified to two particle sizes based on the length of the long axis: <125 μm and >125 μm. When counting charcoal, the number of *Lycopodium* spores was also recorded for calculating charcoal concentration. The formula for calculating charcoal concentration (grains/g) is as follows (Clark and Hussey, 1996):

$$W = (A \times C)/(B \times G)$$

Where: W = Charcoal concentration (grains/g); A = Number of counted charcoal fragments (grains); B = Number of counted *Lycopodium* spores (grains); C = Number of added *Lycopodium* spores (20,630 spores); G = Sample weight (g).

In order to distinguish the sources of fuels (woody vs. herbaceous plants) and the fire event ranges (region vs. local), two distinct charcoal shapes were classified in the identification process by calculating to the ratio of length (major axis) to width (minor axis). If the value was >2.5, the charcoal was classified as sub-long (L) and if the value was <2.5, as sub-round (R) (Figure 3).

3.4 Biological proxies

135 samples, spaced at intervals of 2 cm, were analyzed for biological proxies: total organic carbon (TOC) and organic carbon isotopes (δ13Corg). Approximately 2 g loess per sample, and placed in 80 mL polypropylene centrifuge tubes. In each tube, 20 mL of 2M hydrochloric acid was added, followed by a thorough mixing. After allowing the samples to settle for 24 hours, acid above the sample was discarded by aspiration and distilled water was used for multiple rinses until a neutral pH was achieved. The samples were then placed in an oven and dried at 45°C. Once dried, they were homogenized by grinding with a mortar (Yang et al., 2021) and weighed.

TOC concentration was determined using a Vario EL elemental analyzer, which provides an analytical accuracy of ± 2%. $\delta^{13}C_{org}$ value was analyzed using a MAT253 isotope mass spectrometer (Thermo Fisher Scientific Company). For calibration, blank controls, glutamic acid (USGS-40), and carbon black (GBW04407) were employed. The testing error was maintained below 5%, and the sample recovery rate ranged between 98% and 105%.

Relative abundances of C_3 and C_4 plants were estimated based on the $\delta^{13}C_{org}$ values using an end-member mixed model (Balesdent and Mariotti, 1996). The calculation formula is as follows: C_3 (%) = $[(\delta^{13}C_{org}-\delta^{13}C_{org3})/(\delta^{13}C_{org4}-\delta^{13}C_{org3})]*100$, where $\delta^{13}C_{org}$ represents the total organic carbon isotopic composition of soil, $\delta^{13}C_{org3}$ represents the organic carbon isotope composition of C_3 plants, and $\delta^{13}C_{org4}$ represents the organic carbon isotopic composition of C_4 plants. The average $\delta^{13}C_{org}$ values of C_3 and C_4 plants is often used to calculate their relative abundance directly. The most common $\delta^{13}C_{org}$ value for C_3 plants is around -26‰, while for C_4, it is around -14‰ (Deines, 1980). However, considering the isotopic fractionation (ranging from 1‰ to 3‰), during the process of plant remains forming soil organic matter, we selected -27‰ and -13‰ as the respective $\delta^{13}C_{org}$ values for estimating the relative abundance of C_4 and C_3 plants in the Shengshan Island loess profile.

3.5 Geochemical proxies

Geochemical proxies were collected at each 1-cm interval, totaling 270 samples. Magnetic susceptibility was measured using MS2 magnetic susceptibility meter (Bartington Instrument Company, United Kingdom). The concentrations of Rb and Sr were determined by an x-ray fluorescence spectrophotometer (XRF-1800, made by Shimadzu Company, Japan). Measurement error was less than 5%. The resulting elemental composition is expressed as ppm.

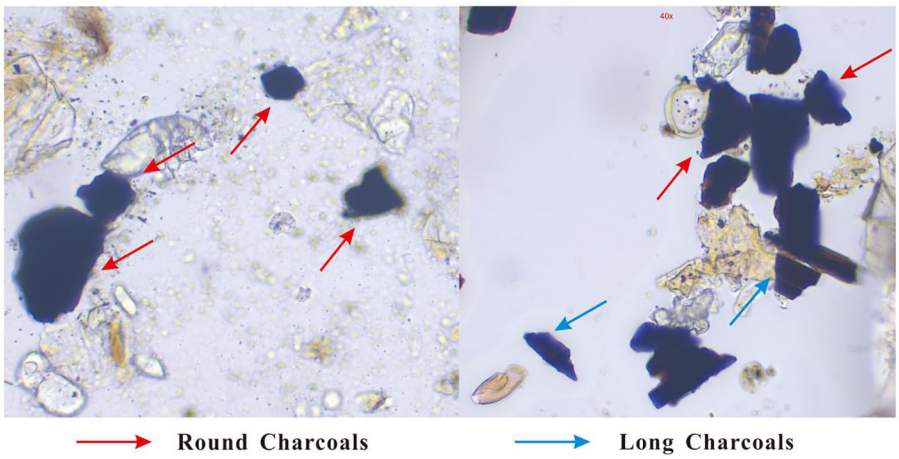

FIGURE 3
Microscope images (40X magnification) of different shapes of charcoal from the Shengshan Island loess profile.

4 Results

4.1 Geochronology

The dating results of the four selected intervals are shown in Table 2. The age of SSD loess profile was estimated to range from 51.67 ± 4 ka (depth: 250 cm) to 0.4 ± 0.1 ka (depth: 10 cm). An age-depth model, illustrating the age at each interval, is depicted in Figure 2, along with the calculated sedimentation rate. Specifically, the sedimentation rate from 51.67 ± 4 ka to 42.41 ± 4 ka (depth 250 to 150 cm) was calculated to be approximately 0.093 cm·ka^{-1}. Subsequently, it increased to over ~ 0.148 cm·ka^{-1} between 42.41 ± 4 ka and 35.03 ± 3 ka (depth 150 to 100 cm). Further, between 35.03 ± 3 ka and 0.40 ± 0.1 ka (depth 100 to 10 cm), the rate escalated to ~ 0.385 cm·ka^{-1}. Loess profiles collected from SSD, including ours, exhibited uniform texture, with no discernible stratigraphic inversions or sedimentation discontinuities (Zheng, 2002; Ren et al., 2022; Wu et al., 2023). Thus, we posit that the profile examined in this study represents continuous deposition, likely occurring during the last glacial period.

4.2 Changes in fire events: evidence from charcoal, biological, and geochemical proxies

4.2.1 Charcoal concentration, particle size, and morphology

Charcoal concentration analysis (Figure 4A) shows that the total charcoal concentration ranged from 2088.8 to 35539.9 grains/g (average: 11282.9 grains/g). Two peaks occured at depths of 20 cm and 270 cm, with values of 31415.7 grains/g and 35539.9 grains/g, respectively. Between these two peaks, the charcoal concentration was much lower (average: 6834 grains/g). The lowest charcoal concentration was 2088.8 grains/g, observed at a depth of 80 cm. The concentration of sub-round charcoal particles ranged from 1860.4 to 327226.7 grains/g (average: 9801.8 grains/g) (Figure 4B), while the concentration of sub-long charcoal particles ranged from 228.4 to 6958.5 grains/g (average: 1489.9 grains/g) (Figure 4C). The trends in total charcoal concentration, as well as concentrations of sub-round and sub-long charcoal particles, were generally consistent, with maximum and minimum values occurring at the same depths.

TABLE 2 OSL (optically stimulated luminescence) dating results of the loess in Shengshan Island.

Sample	Depth (cm)	U (×10^{-6})	Th (×10^{-6})	K (%)	Dose rate (Gy/ka)	De/Gy	Age (ka)
SSD-1	10	2.83 ± 0.10	14.3 ± 0.39	1.49 ± 0.05	3.05 ± 0.20	1.2 ± 0.3	0.40 ± 0.1
SSD-2	100	2.98 ± 0.11	15.1 ± 0.39	1.69 ± 0.06	3.34 ± 0.24	117 ± 4	35.03 ± 3
SSD-3	150	2.94 ± 0.11	14.4 ± 0.39	1.56 ± 0.05	3.23 ± 0.24	137 ± 8	42.41 ± 4
SSD-4	250	2.93 ± 0.11	14.3 ± 0.39	1.62 ± 0.05	3.00 ± 0.20	152 ± 5	51.67 ± 4

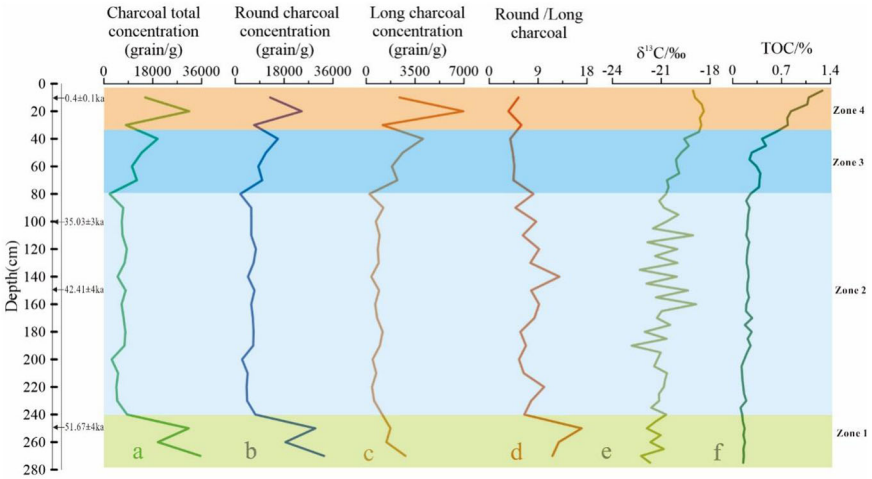

FIGURE 4
Concentration of charcoal in different morphologies of the Shengshan Island loess profile: **(A)** total, **(B)** sub-round, **(C)** sub-long, and **(D)** the sub-round to sub-long ratio. **(E)** $\delta^{13}C_{org}$ and **(F)** TOC values are also indicated.

Regarding charcoal morphology, sub-round charcoal particles dominated throughout the profile (Figure 4B), with an average concentration approximately five times that of sub-long charcoal particles (Figures 4C, 5A). The ratio of sub-round to sub-long charcoal particles ranged from 3.51 to 17, and it showed a generally decreasing trend over time (Figure 4D).

In terms of particle size, the concentration of <125 μm sub-round particle ranged from 1820.1 to 32539.1 grains/g (average: 9661.8 grains/g) (Figure 5B), while >125 μm sub-round particle ranged from 0 to 385.6 grains/g (average: 94.9 grains/g) (Figure 5C). On the other hand, the concentration of <125 μm sub-long particle ranged from 228.3 to 6856.2 grains/g (average: 1478.3 grains/g) (Figure 5B), while >125 μm sub-long particle ranged from 0 to 102.3 grains/g (average: 6.8 grains/g) (Figure 5C). Overall, the total concentration of <125 μm particle ranged from 2048.4 to 35352.3 grains/g (average: 11140.2 grains/g) (Figure 5D). The total concentration of >125μm particle ranged from 14.3 to 409.3 grains/g (average: 120.9 grains/g) (Figure 5E). The trends in charcoal concentration across these two sizes were generally similar to that of the total charcoal concentration (Figure 5A).

4.2.2 Ancient fire dynamics based on the charcoal records

We reconstructed the ancient fire dynamics in the SSD region by analyzing changes in charcoal concentration, particle size, and morphology. We divided the fire history into four distinct zones dating back to the Late Pleistocene. For each zone, we described the frequency of fire events, the vegetation abundance and composition, as well as the geographic extents of these fires.

4.2.2.1 Zone 1 (280-240 cm, 60-50 ka): an epoch of intense fires

Zone 1, corresponding to the mid-Late Pleistocene, was marked by a substantial peak in overall charcoal concentration (Figure 4A), signifying a prevalence of fire incidents during this period. The ratio of <125μm to >125μm was relatively low, suggesting a high frequency of localized fire activities during this stage, with a relatively lower frequency of regional fire activities. Additionally, regarding charcoal morphology, there was a notable peak in the concentration of sub-round charcoal particles (Figure 4B), along with a simultaneous increase in the ratio of sub-round to sub-long charcoal particles (Figure 4D). Since sub-round charcoal particles are indicative of the presence of woody plants (Enache and Cumming, 2006; Thevenon and Anselmetti, 2007; Daniau et al., 2013; Crawford and Belcher, 2014; Leys et al., 2015, Leys et al., 2017), it is likely that the fires mostly combusted woody vegetation during this period.

4.2.2.2 Zone 2 (240-80 cm, 50-30 ka): reduced fire activity

Zone 2, corresponding to the late-Late Pleistocene, exhibited an overall low charcoal concentration (Figure 4A), indicative of fewer fire incidents. The ratio of <125 μm to >125 μm increased compared to Zone 1, with two peaks appearing at 230 cm and 100 cm, respectively. The rise in the ratio signifies a rise in regional fire activities coupled with a decline in localized fire activities. At the same time, notable fluctuations in the ratio imply ongoing variations in the frequencies of both regional and localized fire activities (Figure 5F). According to the charcoal morphology analysis (Figure 4D), the ratio of sub-round to sub-long charcoal particles displayed a fluctuating decreasing trend, suggesting that the relative abundance of herbaceous fuels increased in comparison to zone 1.

4.2.2.3 Zone 3 (80-35 cm, 30-12 ka): increasing fire frequency followed by a sudden decrease

Zone 3, still corresponding to the late-Late Pleistocene, revealed a gradual increase in charcoal concentration followed by a sudden decrease (Figure 4A), indicating a fluctuating fire frequency during this period. The ratio of <125 μm to >125 μm was relatively low, and it remained stable during this stage (Figure 5F). This indicates

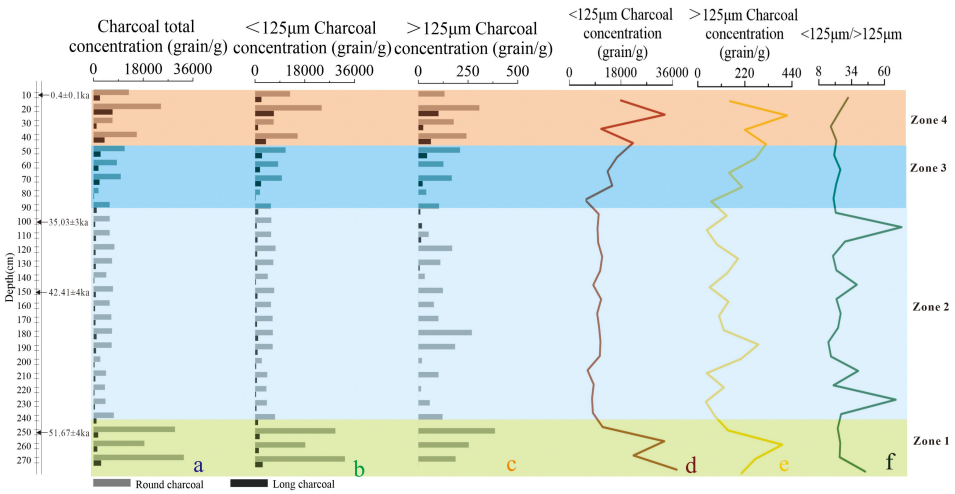

FIGURE 5
Concentration of charcoal in different particle sizes of the Shengshan Island loess profile. Bar graphs (light color: sub-round charcoal; dark color: sub-long charcoal): **(A)** total, **(B)** <125 μm, and **(C)** >125 μm. Trends: **(D)** <125 μm, **(E)** >125 μm, and **(F)** <125 μm to <125 μm ratio.

that there was a higher proportion of localized activities compared to regional activities, suggesting that during this stage, fire activities on Shengshan Island were primarily localized. In the analysis of charcoal morphology (Figure 4D), the ratio of sub-round to sub-long charcoal particles further decreased, indicating a continued shift towards increased burning of herbaceous vegetation.

4.2.2.4 Zone 4 (35-10 cm, 12 ka – present): 2nd surge in fire incidents

Zone 4, corresponding to the Holocene era was marked by a second peak in charcoal concentration (Figure 4A), signifying a resurgence in fire activity. The ratio of <125 μm to >125 μm experienced a slight increase, indicating a rise in regional fire activities during this stage (Figure 5F). In terms of morphology (Figure 4D), the ratio of sub-round to sub-long charcoal particles reached its minimum, suggesting a further increase in the burning of herbaceous vegetation.

4.3 Biological proxies: $\delta^{13}C_{org}$ and TOC

$\delta^{13}C_{org}$ values ranged between -22.82~ -18.39 ‰, with an average of -20.55 ‰. These values (Figure 4E) showed a generally increasing trend: they were lower at the bottom intervals (~ 240-270 cm depth, 60-50 ka), with fluctuations becoming more pronounced in the midsection (~ 240-80 cm depth, 50-30 ka). Subsequently, there was an upward trend in $\delta^{13}C_{org}$ values, persisting until the ~20 cm interval (0.4 ± 0.1 ka), followed by a slight decline in the uppermost layers. TOC levels (Figure 4F) remained relatively stable in most parts of the loess profile, ranging from 0.11 to 1.29%, with an average of 0.31%. Approximately 30 ka ago (~ 80 cm depth), a significant increase began, culminating in the highest TOC concentration at the topmost layer.

4.4 Geochemical proxies: Rb/Sr ratio and magnetic susceptibility

The Rb/Sr ratio (Figure 6E) exhibited an increase trend until reaching ~ 120 cm, experienced a slight declining until ~ 80 cm, and then resumed its descending trend. Magnetic susceptibility (Figure 7F) showed a fluctuating and increasing trend, reaching the minimum and maximum values at ~ 40 cm and ~ 180 cm respectively. The change trend was basically consistent with Rb/Sr.

5 Discussion

5.1 Factors affecting charcoal concentration and particle type

The concentration of charcoal in sediments can be affected by various factors including sedimentation rate, transportation and preservation conditions, and the availability of fuel sources. Hence, it is essential to first assess the potential impact of these factors on charcoal concentration in our SSD loess profile.

5.1.1 Sedimentation rate

Sedimentation rate is negatively related to charcoal concentration: as sedimentation rate increases, charcoal concentration decreases (Vachula and Cheung, 2021; Vachula et al., 2022). In our analysis, we took into account the influence of sedimentation rate on charcoal concentration. Specifically, we adjusted the trend line of charcoal concentration across the entire profile by multiplying it with the sedimentation rate to get the charcoal flux.

Charcoal flux (grains·cm/g·ka) = charcoal concentration (grains/g) * sedimentation rate (cm/ka).

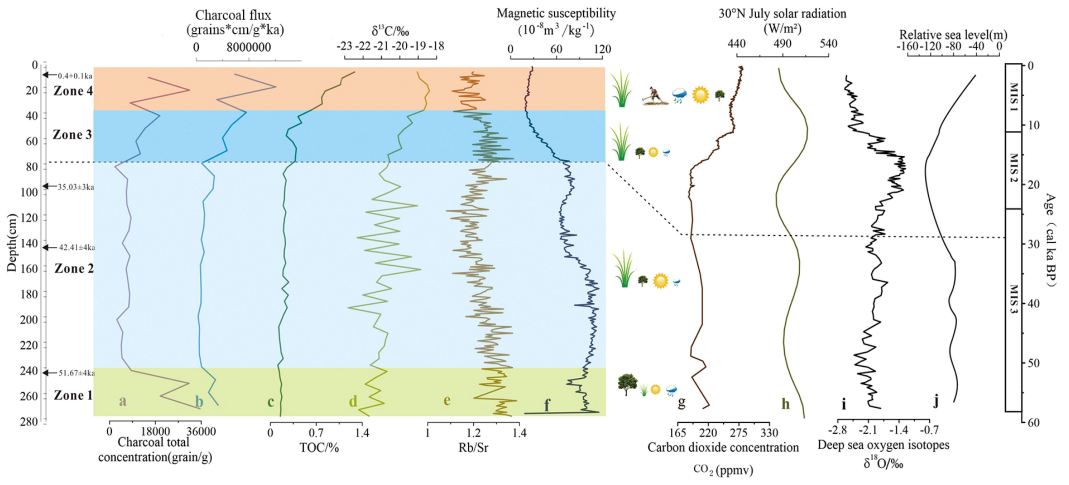

FIGURE 6
Comparison of Shengshan Island loess profile with other global paleoclimatic records: **(A)** charcoal total concentration, **(B)** charcoal flux, **(C)** TOC concentration, **(D)** δ13Corg concentration, **(E)** Rb/Sr ratio, **(F)** magnetic susceptibility, **(G)** carbon dioxide concentration (Monnin et al., 2001; Pépin et al., 2001), **(H)** 30°N July solar radiation (Ding and Liu, 1998), **(I)** deep sea oxygenisotopes (Linsley, 1996), and **(J)** relative sea level (Lambeck et al., 2014).

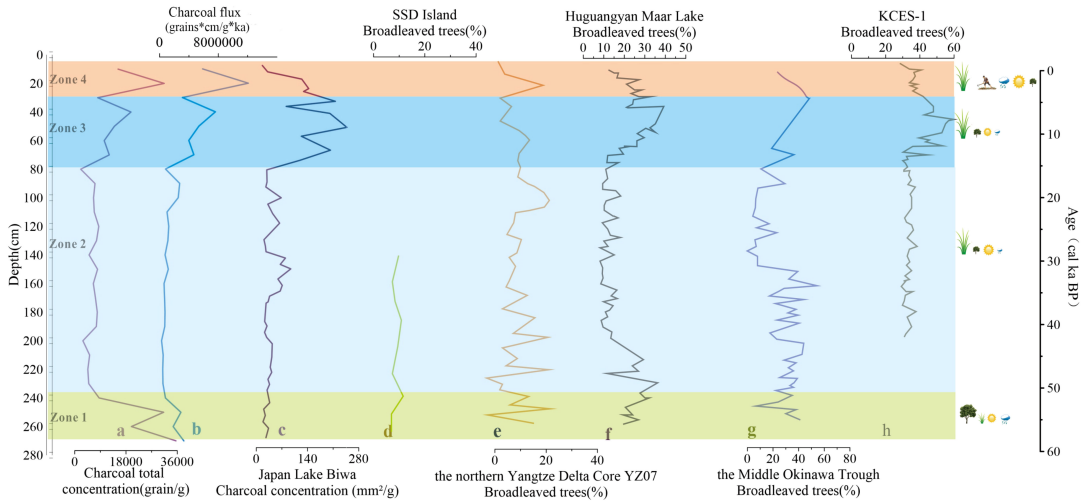

FIGURE 7
Shengshan Island loess profile (**A**: charcoal total concentration, **B**: charcoal flux) compared with other paleoecological records: **(C)** Lake Biwa (Inoue et al., 2018), **(D)** Shengshan Island Profile-2, **(E)** Core YZ07 (Ye et al., 2024), **(F)** HML (Zhang et al., 2020), **(G)** Middle Okinawa Trough (Zheng et al., 2011), and **(H)** KCES-1 (Chen et al., 2017).

The results (Figure 6B) indicated that the sedimentation rate has a discernible impact on charcoal concentration, particularly in zone 1. Originally, zone 1 was thought to have the highest fire frequency, but now it is the 2nd lowest. The trend, after calibration, aligns more closely with other indicators.

5.1.2 Transportation and preservation

Apart from local vegetation combustion, charcoal accumulation can result from water or aeolian transport from nearby regions (Moore et al., 2022). In the transport process, one scenario involves charcoal particles being deposited in the vicinity before being flushed out and transported into low-lying areas by a river, reflecting characteristics of the drainage basin. In the second scenario, particles are carried by strong winds during or after combustion, potentially originating from sources outside the drainage basin. Nevertheless, considering the relationship between the particle size and source distance, the relative transport distance can be assessed: smaller particles are more likely to be transported further by wind or water (Herring, 1985; Clark, 1988; Huang et al., 2006; Turner et al., 2008; Miao et al., 2016, Miao et al., 2017, Miao et al., 2019), regardless of whether they stay within their original drainage basin. The loess profile on SSD has been shown to accumulate through aeolian transportation since the Late Pleistocene (Zheng and Liu, 2006). During that period, the sea level was low (Figure 6J), and the continental shelf was exposed, connecting SSD to the mainland. This implies that wind is the primary factor influencing charcoal accumulation, while the impact of water was negligible.

Charcoal, classified as inertinite, exhibits relative resistance to chemical and microbial decomposition (Eshet et al., 1994; Traverse, 1994; Verardo, 1997; Hockaday et al., 2006; Quénéa et al., 2006). Studies have indicated that preservation does not significantly impact the abundance of charcoal particles in sediments (Moore et al., 2022). During our charcoal extraction process, we observed no discernible relationship between the abundance of charcoal particles and pollen spores, suggesting that preservation was not likely a critical factor influencing charcoal concentration in this analysis.

5.1.3 Fuel sources

Vegetation serves as the primary fuel for fires. Two major photosynthetic mechanisms of terrestrial higher plants are well-documented: the C_3 and C_4 pathways, which generate different carbon isotopic signatures (O'Leary, 1981; Farquhar et al., 1989). C_3 plants include almost all trees and most shrubs, leading to a carbon isotopic composition range between -35‰ and -20 ‰ with an average of about - 26 ‰ (Deines, 1980). The C_4 pathway is characteristic of many savanna grasses and sedges, and produces a carbon isotopic signature range from -16 ‰ to -10 ‰ with an average of -13 ‰ (Deines, 1980).

In our analysis, the $\delta^{13}C_{org}$ results (Figure 4E) exhibited an opposite trend compared to the sub-round to sub-long ratio (Figure 4D): both trends indicate a decrease in the proportion of woody plant combustion over time, with herbaceous plant combustion becoming dominant. This further suggests that the variation in vegetation types (i.e., differences in fuel sources) contributes to changes in charcoal particles and, having a certain impact on fires.

5.2 Driving mechanisms of ancient fire dynamics

5.2.1 Links between fire events, climate, vegetation, and human activities

Climate plays a crucial role in influencing fire events, primarily through variations in temperature and precipitation. To comprehend how climate has impacted fire occurrences in the SSD region, it is

essential to choose reliable indicators that reflect past climate changes. For example, previous studies have demonstrated that a high Rb/Sr ratio is linked to a robust pedogenesis process, suggesting a warm and wet environment (McIntyre et al., 1966). Magnetic susceptibility values can also indicate variations in temperature and precipitation, with higher values typically associated with elevated temperature and precipitation levels (Borradaile, 1988). $\delta^{18}O$ values and solar radiation can also reflect changes in climate: $\delta^{18}O$ values are often negatively related to precipitation (Linsley, 1996), and solar radiation is normally positively associated with temperature (Ding and Liu, 1998).

Vegetation, serving as the essential fuel source for fires, constitutes a significant factor influencing fire events, as elaborated in Section 5.1.3. Research has shown that the $\delta^{13}C_{org}$ value of C_3 plants is often negatively correlated with precipitation (Ehleringer and Cooper, 1988; Diefendorf et al., 2010), indicating that lower $\delta^{13}C_{org}$ values suggest wetter conditions. The TOC content reflects variations in the intensity of bio-pedogenesis during the accumulation of dust and the formation of soil throughout the profile (Gu et al., 1999).

Furthermore, in the last few thousand years, human activities have increasingly impacted fire events. In addition to charcoal particle concentration, CO_2 content is another parameter that directly reflects the extent of fire events. In the following sections, we explore potential interactions between fires, climate, vegetation, and human activities within each of the four phases delineated in the SSD loess profile.

5.2.1.1 Zone 1 (280-240 cm, 60-50 ka): reduced fire frequency after calibration

After calibration, the charcoal concentration of zone 1 became much lower, only slightly higher than that of zone 2, suggesting a low fire frequency. Regarding climate, Rb/Sr ratio, magnetic susceptibility, and solar radiation exhibited relatively high values, while CO_2 and $\delta^{18}O$ values were relatively low (Figure 6), indicating a relatively warm and humid climate. The $\delta^{13}C_{org}$ value during this period was at the lower end, further supporting the humid climate.

Furthermore, the $\delta^{13}C_{org}$ values in this zone fluctuated within the range of -22‰ to -20‰ (average: -21.42 ‰, Figure 6D), likely suggesting the prevalence of C_3 plants (i.e., woody plants) during this mid-Late Pleistocene era on SSD. This aligns with the findings derived from charcoal analysis, which shows a high sub-round to sub-long charcoal particle ratio, indicating the dominance of woody plant combustion (Figure 4D). Additionally, TOC values were generally low during this period, with an average of 0.15% (Figure 6C), suggesting a low biomass and vegetation coverage during this period. Overall, due to the humid climate and scarcity of vegetation, this period experienced a low fire frequency.

5.2.1.2 Zone 2 (240-80 cm, 50-30 ka): remaining low fire frequency

During this period, Rb/Sr ratio and magnetic susceptibility initially decreased and then increased, while solar radiation and $\delta^{18}O$ values fluctuated but remained relatively unchanged (Figure 6), suggesting that the climate was unstable during this period. TOC levels remained low, with an average of ~0.20% (Figure 6C), indicating that the vegetation cover was still limited, likely insufficient to provide substantial fuels for fires. $\delta^{13}C_{org}$ fluctuated dramatically within the range of -21‰ to -19‰ (Figure 6D), suggesting an unstable vegetation assemblage and the fuels were alternating between woody and herbaceous sources, likely caused by the unstable climate. Dramatic changes in temperature and climate induced the alternating status between two different vegetation types, and so the fuels were relatively limited, and reduced the possibility of fire events. The low CO_2 concentration (Figure 6G) further confirms that fire frequency was still low in this period.

5.2.1.3 Zone 3 (80-35 cm, 30-12 ka): increasing fire frequency followed by a sudden decrease

In Zone 3, we observed a rapid decline in Rb/Sr ratio and magnetic susceptibility values, while solar radiation fluctuated and $\delta^{18}O$ values were higher than zone 2 (Figure 6), suggesting a relatively cool and dry climate. Meanwhile, TOC content increased, with an average of 0.39% (Figure 6C), suggesting an increase in biomass. $\delta^{13}C_{org}$ concentration also increased, with an average of -19‰ (Figure 6D), suggesting that the fuel sources were mainly herbaceous plants, consistent with the signal observed in charcoal morphology (Figure 4G). A dry climate with easily combustible herbaceous plants likely induced the elevated fire frequency. CO_2 concentration further confirms that fire events were frequent in this period (Figure 6G).

As for the later period until around 12,000 years ago, there was a sudden decrease in charcoal concentration, and corresponding changes were observed in the climate-indicative vegetation. We speculate that this might be related to certain extreme climate events, with the Younger Dryas (YD) event being the most typical during this period. Therefore, we suspect that events like YD led to a rapid drop in temperature, thereby reducing the fire frequency. However, we cannot rule out the possibility of other contributing factors.

5.2.1.4 Zone 4 (35-10 cm, 12 ka – present): 2nd surge in fire incidents

The Rb/Sr ratio and magnetic susceptibility values exhibited a slight increase, while solar radiation and $\delta^{18}O$ values decreased (Figure 6), indicating a shift to a wetter and warmer climate upon entering the Holocene. There was a substantial increase in the TOC concentration (Figure 6C), with the average rising from 0.39% to 0.97%, suggesting a significant expansion of biomass. Concurrently, $\delta^{13}C_{org}$ values increased (Figure 6D), indicative of herbaceous plant dominance in the vegetation. Historical records (shengsi.gov.cn, n.d.) indicate human inhabitation on SSD since the Neolithic. While specific records of crops during the Neolithic era on Shengshan Island are not available, the Yangtze River Delta in its proximity is renowned as one of the most fertile regions for agriculture in China. The Neolithic era in the Yangtze River Delta and its surrounding areas marked the beginning of crop cultivation, with rice being among the earliest crops cultivated (Kajita et al., 2018; Okazaki et al., 2021). The surge in regional fires (Figure 5F) in this zone likely confirms the increasing impact of human activities from the surrounding areas.

Meanwhile, evidence of early human use of fire emerged in this region during the Neolithic Age: primary functions of fire during this

period included providing warmth, cooking food, repelling wild animals, and fulfilling other survival needs (Hu et al., 2013). Thus, in the context of SSD, we suspect that logging activities for construction and living materials may have contributed to a notable decline in woody plant abundance first. The expansion of agriculture (e.g., rice cultivation) likely led to an increase in herbaceous plant abundance. Throughout this timeframe, the concentration of charcoal experienced sharp rise followed by a subsequent decline, potentially influenced by changes in human activities such as shifts in production practices, lifestyle, and population migration.

5.2.2 Comparison with paleoecological studies from surrounding areas

The source of fuels (i.e., vegetation) is a direct factor causing fires. After charcoal and pollen extraction (done simultaneously), we first tried enumerating the pollens to obtain the vegetation data. However, due to issues such as pollen preservation and the amount of sample used for extraction, the pollen quantity was insufficient to meet statistical standards, resulting in the inability to obtain pollen results. Fortunately, in a recent study conducted in the nearby area of our research (Figure 1C-Profile-2), we increased the sample quantity and successfully conducted pollen analysis. Although, due to differences in profile location and thickness, layers of the same age were only present from 270-150cm, we drew insights from this part of the results (Figure 7D). From the results in Figure 7D, the overall trend in Zone 2 was consistent with the changes in charcoal, indicating the influence of local vegetation type (i.e., fuel) to some extent.

Despite occasionally higher incidence of localized fires on SSD, the main pattern was still characterized by regional fires (i.e., a high proportion of small particles throughout the profile, Figure 5). This suggests that the Shengshan Island loess profile contains information about regional fires, and the partial lack of local vegetation data on Shengshan Island does not seem to have a significant impact on our interpretation of regional fire dynamics.

To further validate the accuracy of our findings, we compared them with results from surrounding areas, including Lake Biwa (Inoue et al., 2018), Core YZ07 (Ye et al., 2024), HML (Zhang et al., 2020), Middle Okinawa Trough (Zheng et al., 2011), KCES-1 (Chen et al., 2017) (Figure 1A, Figure 7). The charcoal concentration curve of Lake Biwa (Figure 7C) is generally consistent with the overall trend of our study's profile. Core YZ07 (Figure 7E), HML (Figure 7F), Middle Okinawa Trough (Figure 7G), KCES-1 (Figure 7H) are woody plant data (relative abundance of broadleaved trees) from pollen analysis conducted in surrounding areas. During Zone 1, the SSD calibrated charcoal concentration curve aligns well with the charcoal concentration curve from Lake Biwa. Additionally, it corresponds to the curve representing the proportion of woody material extracted from the other profile on Shengshan Island (Figure 1C-Profile-2), suggesting that the predominant fuel source was likely woody materials during this period. Zone 2 has the longest duration, and the trends of charcoal concentration across studies showed fluctuations with a generally similar pattern. The woody plant data fluctuated greatly during this stage, and the results for Shengshan Island also indicated a mix of woody and herbaceous fuels. In Zone 3, different studies displayed varying changes, with Core YZ07 showing a decrease in the proportion of woody plants, consistent with our findings. However, other studies showed an increase in the proportion of woody plants, indicating that in regional comparisons, sampling locations closer together have more reference value. In Zone 4, all studies showed a sharp decrease in the proportion of woody plants, in accordance with our finding.

5.3 Connecting the pieces: ancient fire history in the SSD region

During the mid-late Pleistocene (60-50 ka), the SSD region experienced a warm and humid climate with relatively low vegetation coverage, resulting in a low frequency of fires. In the late-Late Pleistocene (50-30 ka), the climate conditions became unstable, with significant temperature and precipitation variations. The drastic climate changes created harsh conditions for plants, contributing to a substantial turnover in plant assemblages and likely a reduction in vegetation coverage. Consequently, this led to limited availability of usable fuel and a lower occurrence of fires during this period.

At the end of the late-Late Pleistocene (30-12 ka), the SSD region experienced reduced precipitation, and the dominant vegetation type shifted to herbaceous plants. The combination of a dry environment and flammable herbaceous plants increased the frequency of fires, and regional fires remained predominant. Towards the end of this period, around 12 ka, there was a sudden decrease in charcoal concentration, corresponding to changes in vegetation proxies indicative of climatic shifts. We speculate that this could be related to extreme climate events (e.g., YD event) that led to a rapid drop in temperature, reducing the occurrence of fires.

Since the beginning of the Holocene (12 ka to the present), the SSD region experienced rising temperatures, and herbaceous plants remained the dominant vegetation type. We suspect that human activities, such as deforestation for construction and living materials, have significantly reduced woody plants. The large-scale cultivation of crops (e.g., rice) altered the composition of vegetation types. During this period, there was a drastic increase and subsequent decrease in charcoal concentration. The reasons for this could be attributed to changes in human production and lifestyle, as well as factors related to population migration. Additionally, there was an increase in regional fires, suggesting the influence of human activities from surrounding areas.

Overall, we successfully reconstructed the ancient fire history in the SSD region over the past millennia and explored the connections between these fires, changes in vegetation, climate, and human activities. Our study contributes to an improved understanding of environmental changes along the Eastern Coast of China since the Late Pleistocene.

Data availability statement

The original contributions presented in the study are included in the article/supplementary material. Further inquiries can be directed to the corresponding authors.

Author contributions

ZW: Conceptualization, Writing – original draft, Writing – review & editing. CW: Methodology, Writing – original draft, Writing – review & editing. YZ: Data curation, Writing – review & editing. YC: Methodology, Writing – review & editing. SR: Data curation, Writing – review & editing. CY: Investigation, Writing – review & editing. HW: Conceptualization, Writing – review & editing. LZ: Supervision, Writing – review & editing. PQ: Supervision, Writing – review & editing. XZ: Conceptualization, Funding acquisition, Resources, Writing – review & editing.

Funding

The author(s) declare financial support was received for the research, authorship, and/or publication of this article. This work was financially supported by the China Natural Science Foundation (Grant Nos. 42371018, 42271027, 41971020) and China Scholarship Council (Grant No. 202206140061). In the end, we also thank the three anonymous reviewers for their constructive comments.

Conflict of interest

The authors declare that the research was conducted in the absence of any commercial or financial relationships that could be construed as a potential conflict of interest.

Publisher's note

All claims expressed in this article are solely those of the authors and do not necessarily represent those of their affiliated organizations, or those of the publisher, the editors and the reviewers. Any product that may be evaluated in this article, or claim that may be made by its manufacturer, is not guaranteed or endorsed by the publisher.

References

Balesdent, J., and Mariotti, A. (1996). Measurement of soil organic matter turnover using 13C natural abundance. *Mass Spectrometry of soils*, 83–111.

Bobek, P., Šamonil, P., and Jamrichová, E. (2018). Biotic controls on Holocene fire frequency in a temperate mountain forest, Czech Republic. *J. Quaternary Sci.* 33, 892–904. doi: 10.1002/jqs.3067

Bond, W. J., and Keeley, J. E. (2005). Fire as a global 'herbivore': the ecology and evolution of flammable ecosystems. *Trends Ecology Evolution* 20, 387–394. doi: 10.1016/j.tree.2005.04.025

Borradaile, G. J. (1988). Magnetic susceptibility, petrofabrics and strain. *Tectonophysics* 156, 1–20. doi: 10.1016/0040-1951(88)90279-X

Bowman, D. M., Balch, J. K., Artaxo, P., Bond, W. J., Carlson, J. M., Cochrane, M. A., et al. (2009). Fire in the earth system. *Science* 324, 481–484. doi: 10.1126/science.1163886

Chen, J., Liu, Y., Shi, X., Suk, B.-C., Zou, J., and Yao, Z. (2017). Climate and environmental changes for the past 44 ka clarified by pollen and algae composition in the Ulleung Basin, East Sea (Japan Sea). *Quaternary Int.* 441, 162–173. doi: 10.1016/j.quaint.2016.09.052

Clark, J. S. (1988). Particle motion and the theory of charcoal analysis: source area, transport, deposition, and sampling. *Quaternary Res* 30, 67–80. doi: 10.1016/0033-5894(88)90088-9

Clark, J. S., and Hussey, T. C. (1996). Estimating the mass flux of charcoal from sedimentary records: effects of particle size, morphology, and orientation. *Holocene* 6, 129–144. doi: 10.1177/095968369600600201

Crawford, A. J., and Belcher, C. M. (2014). Charcoal morphometry for paleoecological analysis: the effects of fuel type and transportation on morphological parameters. *Applications in Plant Sci.* 2, 1400004. doi: 10.3732/apps.1400004

Cui, Q.-Y., Gaillard, M.-J., Lemdahl, G., Sugita, S., Greisman, A., Jacobson, G. L., et al. (2013). The role of tree composition in Holocene fire history of the hemiboreal and southern boreal zones of southern Sweden, as revealed by the application of the Landscape Reconstruction Algorithm: Implications for biodiversity and climate-change issues. *Holocene* 23, 1747–1763. doi: 10.1177/0959683613505339

Daniau, A.-L., Harrison, S., and Bartlein, P. (2010). Fire regimes during the Last Glacial. *Quaternary Sci. Rev.* 29, 2918–2930. doi: 10.1016/j.quascirev.2009.11.008

Daniau, A.-L., Sánchez Goñi, M. F., Martinez, P., Urrego, D. H., Bout-Roumazeilles, V., Desprat, S., et al. (2013). Orbital-scale climate forcing of grassland burning in southern Africa. *Proc. Nat. Acad. Sci.* 110, 5069–5073. doi: 10.1073/pnas.1214292110

Deines, P. (1980). The isotopic composition of reduced organic carbon. *Handbook of environmental isotope geochemistry*. doi: 10.1016/B978-0-444-41780-0.50015-8

Diefendorf, A. F., Mueller, K. E., Wing, S. L., Koch, P. L., and Freeman, K. H. (2010). Global patterns in leaf 13C discrimination and implications for studies of past and future climate. *Proc. Nat. Acad. Sci.* 107, 5738–5743. doi: 10.1073/pnas.0910513107

Ding, Z., and Liu, D. (1998). Forcing mechanisms for East-Asia monsoonal variations during the Late Pleistocene. *Chinese Sci. Bull.* 43, 1497–1510. doi: 10.1007/BF02883437

Durcan, J. A., King, G. E., and Duller, G. A. (2015). DRAC: Dose Rate and Age Calculator for trapped charge dating. *Quaternary Geochronology* 28, 54–61. doi: 10.1016/j.quageo.2015.03.012

Ehleringer, J. R., and Cooper, T. A. (1988). Correlations between carbon isotope ratio and microhabitat in desert plants. *Oecologia* 76, 562–566. doi: 10.1007/BF00397870

Enache, M. D., and Cumming, B. F. (2006). Tracking recorded fires using charcoal morphology from the sedimentary sequence of Prosser Lake, British Columbia (Canada). *Quaternary Res.* 65, 282–292. doi: 10.1016/j.yqres.2005.09.003

Eshet, Y., Habib, D., and Van Pelt, R. (1994). Palynology of sedimentary cycles, Sedimentation of organic particles. *Cambridge Univ. Press* pp, 311–336. doi: 10.1017/CBO9780511524875

Farquhar, G. D., Ehleringer, J. R., and Hubick, K. T. (1989). Carbon isotope discrimination and photosynthesis. *Annu. Review Plant Biol.* 40, 503–537. doi: 10.1146/annurev.pp.40.060189.002443

Gill, A. M. (1977). "Management of fire-prone vegetation for plant species conservation in Australia", 20–26.

Gu, Z., Ding, Z., Xiong, S., and Liu, T. (1999). A seven million geochemical record from Chinese red-clay and loess-paleosol sequence: weathering and erosion in northwestern China. *Quaternary Sci.* 19, 357–365.

Guo, X., Zhao, W., Sun, J., Li, F., Zhang, K., and Zhao, Y. J. (2011). Advances of charcoal study for paleoenvironment in China. *J. Glaciol. Geocryol.* 33, 342–348.

Haberle, S. G., Hope, G. S., and van der Kaars, S. (2001). Biomass burning in Indonesia and Papua New Guinea: natural and human induced fire events in the fossil record. *Palaeogeography Palaeoclimatology Palaeoecol.* 171, 259–268. doi: 10.1016/S0031-0182(01)00248-6

Herring, J. R. (1985). Charcoal fluxes into sediments of the North Pacific Ocean: the Cenozoic record of burning. *Carbon Cycle Atmospheric CO2: Natl. Variations Archean to Present* 32, 419–442. doi: 10.1029/GM032p0419

Hockaday, W. C., Grannas, A. M., Kim, S., and Hatcher, P. G. (2006). Direct molecular evidence for the degradation and mobility of black carbon in soils from ultrahigh-resolution mass spectral analysis of dissolved organic matter from a fire-impacted forest soil. *Organic Geochem.* 37, 501–510. doi: 10.1016/j.orggeochem.2005.11.003

Hoetzel, S., Dupont, L., Schefuß, E., Rommerskirchen, F., and Wefer, G. (2013). The role of fire in Miocene to Pliocene C4 grassland and ecosystem evolution. *Nat. Geosci.* 6, 1027–1030. doi: 10.1038/ngeo1984

Hu, L., Chao, Z., Gu, M., Li, F., Chen, L., Li, X., et al. (2013). Evidence for a Neolithic Age fire-irrigation paddy cultivation system in the lower Yangtze River Delta, China. *J. Archaeol. Sci.* 40, 72–78. doi: 10.1016/j.jas.2012.04.021

Hu, Y., Zhou, B., Pang, Y., and Xu, X. (2019). A review of study methods and progress on hominid use of fire. *Quaternary Sci.* 39, 240–257. doi: 10.11928/j.issn.1001-7410.2019.01.22

Huang, C. C., Pang, J., Su, H., Han, J., Cao, Y., Zhao, W., et al. (2006). Charcoal records of fire history in the Holocene loess–soil sequences over the southern Loess Plateau of China. *Palaeogeography, Palaeoclimatology, Palaeoecology* 239 (1-2), 28–44. doi: 10.1016/j.palaeo.2006.01.004

Hui, Z., Gowan, E. J., Hou, Z., Zhou, X., Ma, Y., Guo, Z., et al. (2021). Intensified fire activity induced by aridification facilitated Late Miocene C4 plant expansion in the northeastern Tibetan Plateau, China. *Palaeogeography, Palaeoclimatology, Palaeoecology* 573, 110437. doi: 10.1016/j.palaeo.2021.110437

Inoue, J., Okuyama, C., and Takemura, K. (2018). Long-term fire activity under the East Asian monsoon responding to spring insolation, vegetation type, global climate, and human impact inferred from charcoal records in Lake Biwa sediments in central Japan. *Quaternary Sci. Rev.* 179, 59–68. doi: 10.1016/j.quascirev.2017.11.007

Jensen, K., Lynch, E. A., Calcote, R., and Hotchkiss, S. C. (2007). Interpretation of charcoal morphotypes in sediments from Ferry Lake, Wisconsin, USA: do different plant fuel sources produce distinctive charcoal morphotypes? *The Holocene* 17, 907–915. doi: 10.1177/0959683607082405

Kajita, H., Kawahata, H., Wang, K., Zheng, H., Yang, S., Ohkouchi, N., et al. (2018). Extraordinary cold episodes during the mid-Holocene in the Yangtze delta: Interruption of the earliest rice cultivating civilization. *Quaternary Sci. Rev.* 201, 418–428. doi: 10.1016/j.quascirev.2018.10.035

Lai, Z. (2006). Testing the use of an OSL standardised growth curve (SGC) for De determination on quartz from the Chinese Loess Plateau. *Radiation Measurements* 41, 9–16. doi: 10.1016/j.radmeas.2005.06.031

Lambeck, K., Rouby, H., Purcell, A., Sun, Y., and Sambridge, M. (2014). Sea level and global ice volumes from the Last Glacial Maximum to the Holocene. *Proc. Natl. Acad. Sci.* 111 (43), 15296–15303. doi: 10.1073/pnas.1411762111

Leys, B., Brewer, S. C., McConaghy, S., Mueller, J., and McLauchlan, K. K. (2015). Fire history reconstruction in grassland ecosystems: amount of charcoal reflects local area burned. *Environmental Res. Lett.* 10 (11), 114009. doi: 10.1088/1748-9326/10/11/114009

Leys, B., and Carcaillet, C. (2016). Subalpine fires: the roles of vegetation, climate and, ultimately, land uses. *Climatic Change* 135, 683–697. doi: 10.1007/s10584-016-1594-4

Leys, B. A., Commerford, J. L., and McLauchlan, K. K. (2017). Reconstructing grassland fire history using sedimentary charcoal: Considering count, size and shape. *PLoS One* 12 (4), e0176445. doi: 10.1371/journal.pone.0176445

Leys, B. A., Marlon, J. R., Umbanhowar, C., and Vannière, B. (2018). Global fire history of grassland biomes. *Ecol. Evol.* 8, 8831–8852. doi: 10.1002/ece3.4394

Lian, L. (2019). The natural fire history during warming periods of Cenozoic. *Quaternary Sci.* 39, 1289–1296. doi: 10.11928/j.issn.1001-7410.2019.05.20

Linsley, B. K. (1996). Oxygen-isotope record of sea level and climate variations in the Sulu Sea over the past 150,000 years. *Nature* 380 (6571), 234–237. doi: 10.1038/380234a0

Liu, L., Cheng, T., Wu, C., Ren, S., Zhou, L., and Zheng, X. (2020). Hematite and goethite content in the dust deposition from the eastern islands of the Yangtze River Delta and its paleoclimatic significance. *Acta Sedimentologica Sinica* 2020, 518–527.

Lv, J., Wang, Y., and Li, C. J. (2002). Fossil charcoal and ancient forest fire. *J.Palaeogeography* 4 (02), 71–76.

MacDonald, G. M., Larsen, C. P., Szeicz, J. M., and Moser, K. A. (1991). The reconstruction of boreal forest fire history from lake sediments: a comparison of charcoal, pollen, sedimentological, and geochemical indices. *Quaternary Sci. Rev.* 10 (1), 53–71. doi: 10.1016/0277-3791(91)90030-X

Maher, L. Jr. (1981). Statistics for microfossil concentration measurements employing samples spiked with marker grains. *Rev. Palaeobotany Palynology* 32 (2-3), 153–191. doi: 10.1016/0034-6667(81)90002-6

McElwain, J. (1998). Do fossil plants signal palaeoatmospheric carbon dioxide concentration in the geological past? *Philosophical Transactions Royal Soc. London. Series B: Biological Sci.* 353(1365), 83–96. doi: 10.1098/rstb.1998.0193

McIntyre, G., Brooks, C., Compston, W., and Turek, A. J. (1966). The statistical assessment of Rb-Sr isochrons. *J. Geophysic. Res.* 71 (22), 5459–5468. doi: 10.1029/JZ071i022p05459

Miao, Y., Jin, H., and Cui, J. (2016). Human activity accelerating the rapid desertification of the Mu Us Sandy Lands, North China. *Scientific Rep.* 6, 23003. doi: 10.1038/srep23003

Miao, Y., Wu, F., Warny, S., Fang, X., Lu, H., Fu, B., et al. (2019). Miocene fire intensification linked to continuous aridification on the Tibetan Plateau. *Geology* 47 (4), 303–307. doi: 10.1130/G45720.1

Miao, Y., Zhang, D., Cai, X., Li, F., Jin, H., Wang, Y., et al. (2017). Holocene fire on the northeast Tibetan Plateau in relation to climate change and human activity. *Quaternary Int.* 443, 124–131. doi: 10.1016/j.quaint.2016.05.029

Millspaugh, S. H., and Whitlock, C. (1995). A 750-year fire history based on lake sediment records in central Yellowstone National Park, USA. *Holocene* 5 (3), 283–292. doi: 10.1177/095968369500500303

Min, W., Hongwei, M., Linpei, H., Qifa, S., Hucai, Z., and Caiming, S. (2020). Vegetation succession and forest fires over the past 13000 years in the catchment of Yangzonghai Lake, Yunnan. *Quaternary Sci.* 40, 175–189. doi: 10.11928/j.issn.1001-7410.2020.01.17

Molinari, C., Carcaillet, C., Bradshaw, R. H., Hannon, G. E., and Lehsten, V. (2020). Fire-vegetation interactions during the last 11,000 years in boreal and cold temperate forests of Fennoscandia. *Quaternary Sci. Rev.* 241, 106408. doi: 10.1016/j.quascirev.2020.106408

Monnin, E., Indermühle, A., Daüllenbach, A., Flückiger, J., Stauffer, B., Stocker, T. F., et al. (2001). Atmospheric CO2 concentrations over the last glacial termination. *Science* 291, 112–114. doi: 10.1126/science.291.5501.112

Moore, H. R., Crocker, A. J., Belcher, C. M., Meckler, A. N., Osborne, C. P., Beerling, D. J., et al. (2022). Hydroclimate variability was the main control on fire activity in northern Africa over the last 50,000 years. *Quaternary Sci. Rev.* 288, 107578. doi: 10.1016/j.quascirev.2022.107578

Murray, A. S., and Wintle, A. G. (2000). Luminescence dating of quartz using an improved single-aliquot regenerative-dose protocol. *Radiat. Measurements* 32, 57–73. doi: 10.1016/S1350-4487(99)00253-X

Nakagawa, T., Brugiapaglia, E., Digerfeldt, G., Reille, M., BEAULIEU, J. L. D., and Yasuda, Y. (1998). Dense-media separation as a more efficient pollen extraction method for use with organic sediment/deposit samples: comparison with the conventional method. *Boreas* 27 (1), 15–24. doi: 10.1111/j.1502-3885.1998.tb00864.x

Okazaki, K., Takamuku, H., Kawakubo, Y., Hudson, M., and Chen, J. (2021). Cranial morphometric analysis of early wet-rice farmers in the Yangtze River Delta of China. *Anthropological Sci.* 129, 203–222. doi: 10.1537/ase.210325

O'Leary, M. H. (1981). Carbon isotope fractionation in plants. *Phytochemistry* 20 (4), 553–567. doi: 10.1016/0031-9422(81)85134-5

Patterson, W. A.III, Edwards, K. J., and Maguire, D. J. (1987). Microscopic charcoal as a fossil indicator of fire. *Quaternary Sci. Rev.* 6, 3–23. doi: 10.1016/0277-3791(87)90012-6

Pépin, L., Raynaud, D., Barnola, J. M., and Loutre, M. J. (2001). Hemispheric roles of climate forcings during glacial-interglacial transitions as deduced from the Vostok record and LLN-2D model experiments. *J. Geophysical Res.: Atmospheres* 106 (D23), 31885–31892. doi: 10.1029/2001JD900117

Pereboom, E. M., Vachula, R. S., Huang, Y., and Russell, J. (2020). The morphology of experimentally produced charcoal distinguishes fuel types in the Arctic tundra. *The Holocene* 30 (7), 1091–1096. doi: 10.1177/0959683620908629

Power, M. J., Marlon, J., Ortiz, N., Bartlein, P. J., Harrison, S. P., Mayle, F. E., et al. (2008). Changes in fire regimes since the Last Glacial Maximum: an assessment based on a global synthesis and analysis of charcoal data. *Climate Dynamics* 30 (7-8), 887–907. doi: 10.1007/s00382-007-0334-x

Qian, P., Zheng, X.-m., Cheng, J., Han, Y.-j., Dong, Y., and Zhang, J.-g. (2018). Tracing the provenance of aeolian loess in the Yangtze River Delta through zircon U–Pb age and geochemical investigations. *J. Mountain Sci.* 15 (4), 708–721. doi: 10.1007/s11629-017-4437-5

Quénéa, K., Derenne, S., Rumpel, C., Rouzaud, J.-N., Gustafsson, O., Carcaillet, C., et al. (2006). Black carbon yields and types in forest and cultivated sandy soils (Landes de Gascogne, France) as determined with different methods: Influence of change in land use. *Organic Geochemistry* 37 (9), 1185–1189. doi: 10.1016/j.orggeochem.2006.05.010

Ramanathan, V., Crutzen, P. J., Kiehl, J., and Rosenfeld, D. (2001). Aerosols, climate, and the hydrological cycle. *Science* 294, 2119–2124. doi: 10.1126/science.1064034

Ren, S., Zheng, X., Zhou, L., Lü, H., Ai, D., Xuan, X., et al. (2018). Analysis of environmentally sensitive grain-size component of loess on the Shengshan Island in East China Sea Based on Optically Stimulated Luminescence Dating. *Quaternary Sci.* 38, 646–658. doi: 10.11928/j.issn.1001-7410.2018.03.09

Ren, S., Song, Y., Long, H., Wu, C., Wang, Z., Yi, C., et al. (2022). Records of Organic Carbon Isotopic Composition and Its Paleoenvironmental Implications in Shengshan Island Loess Deposition in the East China Sea during the Last Glacial Period. *Applied Sciences* 12 (11), 5724.

Santín, C., Doerr, S. H., Kane, E. S., Masiello, C. A., Ohlson, M., de la Rosa, J. M., et al. (2016). Towards a global assessment of pyrogenic carbon from vegetation fires. *Global Change Biol.* 22, 76–91. doi: 10.1111/gcb.12985

Scott, A. C., and Glasspool, I. (2006). The diversification of Paleozoic fire systems and fluctuations in atmospheric oxygen concentration. *Proc. Natl. Acad. Sci.* 103 (29), 10861–10865. doi: 10.1073/pnas.0604090103

Shi, Y., Pan, B., Wei, M., Li, X., Cai, M., Wang, J., et al. (2020). Wildfire evolution and response to climate change in the Yinchuan Basin during the past 1.5 Ma based on the charcoal records of the PL02 core. *Quaternary Sci. Rev.* 241, 106393. doi: 10.1016/j.quascirev.2020.106393

Siegenthaler, U., Stocker, T. F., Monnin, E., Luthi, D., Schwander, J., Stauffer, B., et al. (2005). Stable carbon cycle climate relationship during the Late Pleistocene. *Science* 310 (5752), 1313–1317. doi: 10.1126/science.1120130

Stockmarr, J. (1971). Tables with spores used in absolute pollen analysis. *Pollen et Spores* 13, 615–621.

Tan, Z., Huang, C. C., Pang, J., and Zhou, Q. (2011). Holocene wildfires related to climate and land-use change over the Weihe River Basin, China. *Quaternary International* 234 (1-2), 167–173. doi: 10.1016/j.quaint.2010.03.008

Thevenon, F., and Anselmetti, F. S. (2007). Charcoal and fly-ash particles from Lake Lucerne sediments (Central Switzerland) characterized by image analysis: anthropologic, stratigraphic and environmental implications. *Quaternary Sci. Rev.* 26 (19-21), 2631–2643. doi: 10.1016/j.quascirev.2007.05.007

Traverse, A. (1994). *Sediment. Org. Particles*. doi: 10.1017/CBO9780511524875

Turner, R., Roberts, N., Jones, M. J. G., and Change, P. (2008). Climatic pacing of Mediterranean fire histories from lake sedimentary microcharcoal. *Global and Planetary Change* 63 (4), 317–324. doi: 10.1016/j.gloplacha.2008.07.002

Umbanhowar, C. E. Jr., and Mcgrath, M. (1998). Experimental production and analysis of microscopic charcoal from wood, leaves and grasses. *Holocene* 8 (3), 341–346. doi: 10.1191/095968398666496051

Vachula, R., and Cheung, A. (2021). Late Neogene surge in sedimentary charcoal fluxes partly due to preservation biases, not fire activity. *Palaeogeography Palaeoclimatology Palaeoecol.* 567, 110273. doi: 10.1016/j.palaeo.2021.110273

Vachula, R. S., Sheppard, R. Y., and Cheung, A. H. (2022). Preservation biases are pervasive in Holocene paleofire records. *Palaeogeography Palaeoclimatology Palaeoecol.* 602, 111165. doi: 10.1016/j.palaeo.2022.111165

Verardo, D. (1997). Charcoal analysis in marine sediments. *Limnology and Oceanography* 42 (1), 192–197. doi: 10.4319/lo.1997.42.1.0192

Wang, Z., Miao, Y., Zhao, Y., Li, F., Lei, Y., Xiang, M., et al. (2020). Characteristics of microcharcoal in the lake surface sediments in the northern margin of Qaidam Basin of China and its environmental significance. *J. Desert Res.* 40 (4), 10.

Whitlock, C., Shafer, S. L., and Marlon, J. (2003). The role of climate and vegetation change in shaping past and future fire regimes in the northwestern US and the implications for ecosystem management. *For. Ecol. Manage.* 178, 5–21. doi: 10.1016/S0378-1127(03)00051-3

Wu, C., Wang, Z., Wang, Q., Qian, P., Zheng, X., and Wei, G. (2023). Sedimentary provenance and age of the Shengshan Island loess on the continental shelf of the East China Sea: Implications for windblown dust transport during the Last Glaciation. *Geomorphology* 427, 108624. doi: 10.1016/j.geomorph.2023.108624

Xin, X., and Yiyin, L. (2015). Comparison of the fire history reconstructions from three different kinds of charcoal data on the same site, Daxing'an Mountain. *Quaternary Sci.* 35 (4), 960–966. doi: 10.11928/j.issn.1001-7410.2015.04.17

Xue, J., Zhong, W., Li, Q., Cheng, R., You, A., Wei, Z., et al. (2018). Holocene fire history in eastern monsoonal region of China and its controls. *Palaeoclimatology Palaeoecol.* 496, 136–145. doi: 10.1016/j.palaeo.2018.01.029

Yang, S., Liu, L., Chen, H., Tang, G., Luo, Y., Liu, N., et al. (2021). Variability and environmental significance of organic carbon isotopes in Ganzi loess since the last interglacial on the eastern Tibetan Plateau. *Catena* 196, 104866. doi: 10.1016/j.catena.2020.104866

Ye, L., Gao, L., Han, M., Li, Y., Xiao, X., and Long, H. (2024). The late Quaternary palynological record of the northern Yangtze Delta: Implication for palaeoclimate change in East Asia. *Catena* 234, 107630. doi: 10.1016/j.catena.2023.107630

Zhang, J., Lu, H., Jia, J., Shen, C., Wang, S., Chu, G., et al. (2020). Seasonal drought events in tropical East Asia over the last 60,000 y. *Proc. Natl. Acad. Sci.* 117, 30988–30992. doi: 10.1073/pnas.2013802117

Zheng, X. (2002). Phytilth and its Paleoenvironmental significance in aeolian loess of Shengshan Island of the East China Sea. *Mar. Geol. Quaternary Geol.* 22, 26–30.

Zheng, X., and Liu, F. (2006). Review of reseach on loess in the yangtze river delta and the East China sea islands. *J. -East China Normal Univ. Nat. Sci.* 6 (130), 9.

Zheng, Z., Yang, S., Deng, Y., Huang, K., Wei, J., Berne, S., et al. (2011). Pollen record of the past 60 ka BP in the Middle Okinawa Trough: Terrestrial provenance and reconstruction of the paleoenvironment. *Palaeogeography Palaeoclimatology Palaeoecol.* 307, 285–300. doi: 10.1016/j.palaeo.2011.05.026